

## Article

# The Hazards Analysis of Nickel-Rich Lithium-Ion Battery Thermal Runaway under Different States of Charge

Kun Jiang, Pingwei Gu, Peng Huang, Ying Zhang, Bin Duan \*  and Chenghui Zhang 

School of Control Science and Engineering, Shandong University, Jinan 250061, China; 201934452@mail.sdu.edu.cn (K.J.); gpwei@mail.sdu.edu.cn (P.G.); huangpeng19970119@163.com (P.H.); yzhang03@mail.sdu.edu.cn (Y.Z.); zchui@sdu.edu.cn (C.Z.)

\* Correspondence: duanbin@sdu.edu.cn; Tel.: +86-158-6674-1354

**Abstract:** The lithium-ion battery industry has been developing rapidly, with energy density and capacity constantly improving. However, the ensuing safety accidents of lithium-ion power batteries have seriously threatened the personal safety of passengers. Therefore, more and more attention has been paid to the thermal safety research of lithium-ion batteries, such as thermal runaway (TR) mechanism analysis and prevention methods, etc. In this paper, the nickel-rich 18650 lithium-ion batteries with  $\text{Li}[\text{Ni}_{0.8}\text{Co}_{0.1}\text{Mn}_{0.1}]\text{O}_2$  cathode in different states of charge (SOC) are taken to investigate the TR characteristics using an extended volume plus acceleration calorimeter (EV+-ARC). In order to evaluate the TR characteristics, some characteristic parameters such as battery voltage, surface temperature, temperature rise rate, etc. are selected from the experiment to analyze the influence of SOC on the critical state of TR. It can be seen from the experiment results that the maximum temperature of the battery surface decreases with the decrease of SOC, while the self-generated heat temperature and TR trigger temperature increases with the decrease of SOC.

**Keywords:** thermal runaway; lithium-ion batteries; state of charge; extended volume plus-accelerating rate calorimetry



check for updates

**Citation:** Jiang, K.; Gu, P.; Huang, P.; Zhang, Y.; Duan, B.; Zhang, C. The Hazards Analysis of Nickel-Rich Lithium-Ion Battery Thermal Runaway under Different States of Charge. *Electronics* **2021**, *10*, 2376. <https://doi.org/10.3390/electronics10192376>

Academic Editor: Stanimir Valtchev

Received: 1 September 2021

Accepted: 27 September 2021

Published: 28 September 2021

**Publisher's Note:** MDPI stays neutral with regard to jurisdictional claims in published maps and institutional affiliations.



**Copyright:** © 2021 by the authors. Licensee MDPI, Basel, Switzerland. This article is an open access article distributed under the terms and conditions of the Creative Commons Attribution (CC BY) license (<https://creativecommons.org/licenses/by/4.0/>).

## 1. Introduction

In recent years, with the continuous increase in the use of fossil fuels, the energy crisis and environmental pollution have become more and more serious. In addition, the implementation of green new energy has been strongly advocated in the global scope. The lithium-ion batteries are a new type of green energy storage device, which have the characteristics of high energy density, low self-discharge, long cycle life, etc. [1–3]. Therefore, the application of lithium-ion batteries in various electronic products and electric vehicles (EVs) has attracted extensive attention and developed rapidly [4]. In order to meet the needs of electric vehicles and energy storage, people increase the energy density of the batteries through optimizing their structure and research new materials. At present, the battery structure has basically been optimized to the limit, thus only through the development of new materials with high capacity and high safety [5].

It is well known that the capacity of lithium-ion batteries mainly depends on the cathode material inside the battery. The development of cathode materials with high specific capacity is one of the most effective ways to improve the energy density of lithium-ion batteries. At present, the common cathode materials for lithium-ion batteries on the market mainly include  $\text{LiCoO}_2$  (LCO),  $\text{LiMnO}_2$  (LMO),  $\text{LiFePO}_4$  (LFP),  $\text{LiNi}_x\text{Co}_y\text{Mn}_z\text{O}_2$  (NCM), etc. [6,7]. Compared with other materials, the NCM cathode can achieve higher specific capacity. The larger the value of  $x$ , the greater the specific capacity. Therefore, for the purpose of increasing the battery energy density, the nickel-rich NCM cathode materials such as  $\text{Li}[\text{Ni}_{0.6}\text{Co}_{0.2}\text{Mn}_{0.2}]\text{O}_2$  (NCM622),  $\text{Li}[\text{Ni}_{0.8}\text{Co}_{0.1}\text{Mn}_{0.1}]\text{O}_2$  (NCM811), etc. are researched after  $\text{Li}[\text{Ni}_{1/3}\text{Co}_{1/3}\text{Mn}_{1/3}]\text{O}_2$  (NCM111) [8,9]. However, as the energy density continues to increase, the thermal stability of the battery gets lower and lower. Similar to most cathode

materials, it will decompose and release large quantities of oxygen at high temperatures. Then, this oxygen will react with other materials such as an electrolyte, thereby generating a lot of heat in the battery. When the generated gas and heat cannot be fully discharged or once a battery with a higher energy density enters the thermal runaway (TR), it will inevitably cause more serious damage such as fire and explosion [10–13]. Therefore, it is of great significance for the progress of EVs to carry out research on the TR harms of high energy density lithium-ion batteries.

Safety issues such as the TR of lithium-ion batteries are attracting more and more attention. In order to comprehensively analyze the mechanism and inducement of lithium-ion battery TR, a great deal of native and foreign researchers have made a suite of studies on this issue. Can-Yong Jhu et al. used the adiabatic calorimeter vent sizing package 2 (VSP2) to study the adiabatic TR reaction of commercial  $\text{LiCoO}_2$  lithium-ion batteries from different manufacturers, to determine their thermal instability and adiabatic TR characteristics. Then, the thermal kinetic parameters of the lithium-ion battery reaction were determined using the Arrhenius formula [14]. Feng et al. used the extended volume acceleration rate calorimeter (EV-ARC) and differential scanning calorimeter (DSC) to study the TR mechanism and characteristics of large format prismatic lithium-ion batteries [15,16]. The early studies of Wang et al. found the thermal stability of lithium-ion battery materials through the C80 micro calorimeter and EV-ARC. Moreover, the internal short circuit under different conditions was researched through nail penetration experiments, and a micro-short circuit structure was proposed to explain the mechanism of the internal short circuit [17–19]. Ren et al. proposed an electrochemical-thermal coupled overcharge-thermal runaway model to predict the thermal behavior of lithium-ion batteries at overcharge conditions. A series of overcharge experiments were carried out using EV-ARC to verify the rationality of the model. In addition, the key parameters were further modeled and analyzed, which provided the possibility to solve the overcharge problem of lithium-ion batteries [20]. Liu et al. established a thermal abuse reaction model based on the  $\text{LiNi}_{0.8}\text{Co}_{0.1}\text{Mn}_{0.1}\text{O}_2/\text{SiO}_x\text{-C}$  system with the aid of a differential scanning calorimetry and acceleration rate calorimeter. The model was extended to compare batteries with different laminated numbers and electrode sizes on the internal short circuit issue [21]. Although these representative studies provide a good reference for the study of lithium-ion battery TR. However, there are few researches on the TR of nickel-rich lithium-ion batteries under different state of charge (SOC) conditions. The harm of the TR of lithium-ion batteries under different SOC conditions is not clear.

In this paper, the nickel-rich 18650 lithium-ion batteries with the  $\text{Li}[\text{Ni}_{0.8}\text{Co}_{0.1}\text{Mn}_{0.1}]\text{O}_2$  cathode in different SOC conditions are taken to investigate the TR characteristics using the extended volume plus acceleration calorimeter (EV+-ARC). In order to evaluate the TR characteristics, some characteristic parameters such as battery voltage, surface temperature, temperature rise rate, etc. are selected from the experiment to analyze the influence of SOC on the critical state of TR. Based on the experimental data, combined with the battery mass, specific heat capacity, and transient temperature distribution, the total energy and TNT equivalent value in the process of adiabatic TR is calculated.

## 2. Experiment

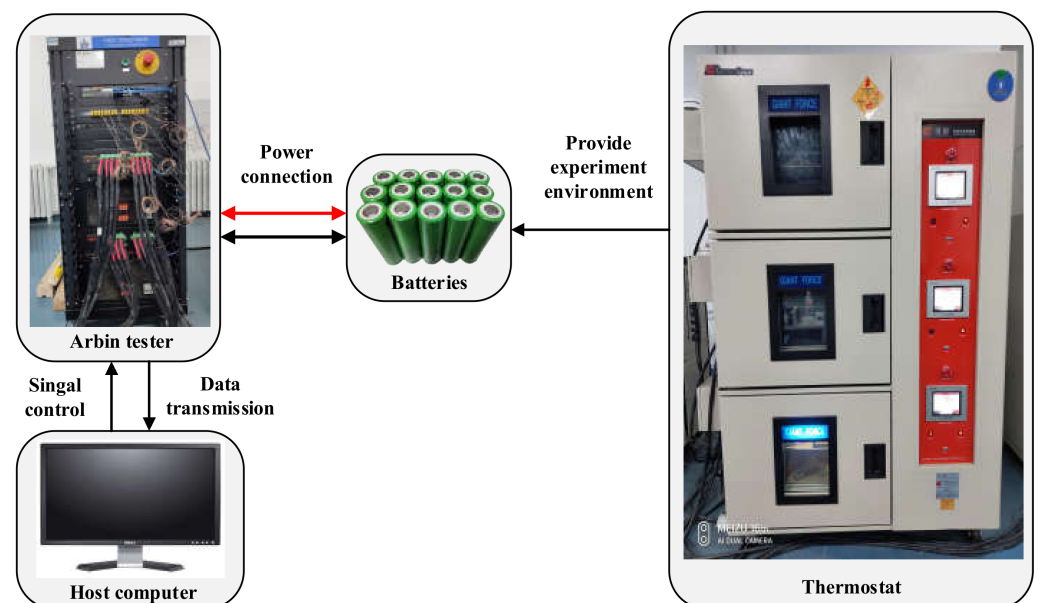
### 2.1. Battery Samples and the SOC Method

The research samples in this paper are  $\text{Li}[\text{Ni}_{0.8}\text{Co}_{0.1}\text{Mn}_{0.1}]\text{O}_2$  cathode 18650 lithium-ion batteries (LG INR18650MJ1), a new type of nickel-rich high-capacity lithium-ion battery, with a diameter of 18.0 mm and length of 65.0 mm. The anode materials are silicon-graphite, and the electrolyte is the  $\text{LiPF}_6$  based solution. The nominal capacity of the battery sample is 3350 mAh, the nominal voltage is 3.7 V, the weight is 47 g, and the working voltage range is 2.5 to 4.2 V. The parameters of the battery samples are shown in Table 1.

**Table 1.** The parameters of the battery samples.

Parameter	Value
Length (mm)	65.1
Diameter (mm)	18.5
Surface area (m <sup>2</sup> )	0.0043
Volume (m <sup>3</sup> )	$1.75 \times 10^{-5}$
Mass (g)	47
Nominal capacity (mAh)	3350
Nominal voltage (V)	3.635
Charge and discharge cut-off voltage (V)	2.5–4.2

The experimental platform for lithium-ion batteries testing is shown in Figure 1, which is mainly composed of three parts: The Arbin battery test system (BT-5HC 5V-60A) for battery charging and discharging, the host computer for programming and saving experimental data, and the thermostat used to control the temperature. Firstly, the new battery was performed three times using the experimental platform, including the constant current-constant voltage (CC-CV) charging and constant current discharging. The current during constant current charging and discharging is  $1/3C$ , where  $1C$  denotes that the current is equal to the nominal capacity in value. The  $C/3$  (1.1A) charging and discharging curves of the lithium-ion battery are shown in Figure 2. Then, the batteries are respectively charged to the specific SOCs with a  $1/3C$  constant current: 0%, 25%, 50%, 75%, and 100% (fully charged). All the experiments are carried out in the thermostat at 25 °C.

**Figure 1.** The experimental platform for charging and discharging.

## 2.2. Thermal Runaway Experiment

In this study, the thermal runaway experiments are all carried out in the extended volume plus accelerated rate calorimeter (EV+-ARC) produced by the THT Company (London, Britain), as shown in Figure 3, which is the latest product. Its volume is much larger than EV-ARC and the other calorimeters, which is more suitable for batteries' safety experiments such as TR. In the study of batteries' thermal safety, the temperature rise ( $\delta T$ ) and energy ( $\delta Q$ ) can be linked through the specific heat capacity of the battery, as shown in (1). Therefore, before conducting the thermal runaway experiment of the batteries with different states of charge, the specific heat capacity of the battery is measured using the direct current (DC) constant current source and EV+-ARC. The polyamide heater is placed in the middle of the three batteries to ensure the batteries are heated evenly, and then it is

placed in the calorimeter, as shown in Figure 4. After the EV+-ARC enters the adiabatic mode, the batteries are heated using the constant current source. The specific heat capacity of the batteries is 1020 J/kg/K, which is calculated by (2).

$$\delta Q = MC_p \delta T \quad (1)$$

$$c_p = \frac{p}{m} \cdot \frac{1}{dT/dt} \quad (2)$$

In order to find the possible heat release behavior of the battery, the EV+-ARC is operated in the heat-wait-seek (H-W-S) mode during the TR experiment. First, the battery is heated from the ambient temperature to 45 °C, and then the temperature is increased in steps of 5 °C every 45 min until the algorithm detects that the sensitivity of the exothermic reaction rate of the battery is greater than 0.02 °C/min. At this point, EV+-ARC turns into an exothermic mode and the calorimeter tracks the temperature change of the battery. The temperature of the battery rises due to the self-heating reaction until the TR occurs. The battery is suspended in the calorimeter, and the thermocouple is pasted on the surface of the battery. The voltage change of the battery is synchronously monitored by a voltage acquisition device produced by Qingdao MKL Co., Ltd. (Qindao, China), The schematic diagram of the TR experiment is shown in Figure 5.

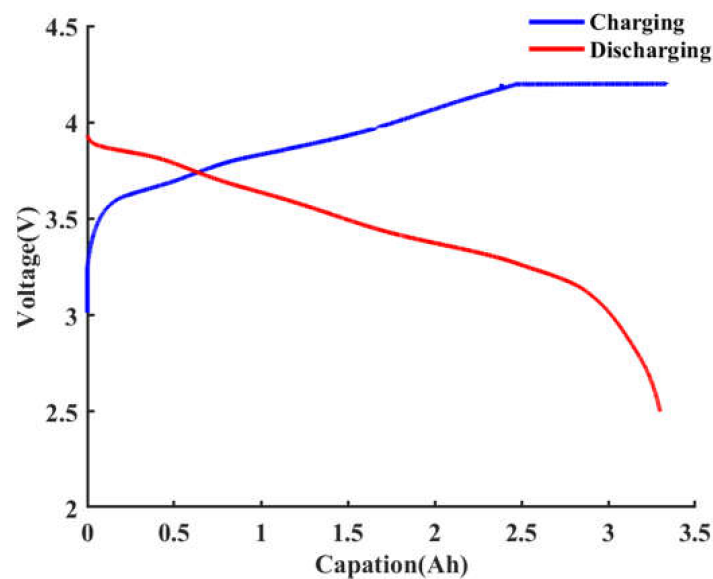


Figure 2. The charging and discharging curves of the battery.



Figure 3. The experimental platform for charging and discharging.



Figure 4. The specific heat capacity experiment.

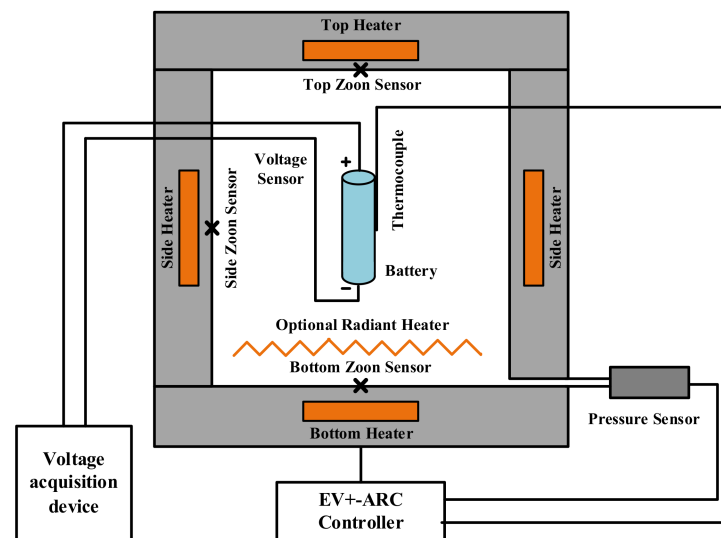


Figure 5. The schematic diagram of the TR experiment.

### 3. Results and Discussion

#### 3.1. Temperature and Voltage Change in TR Experiments

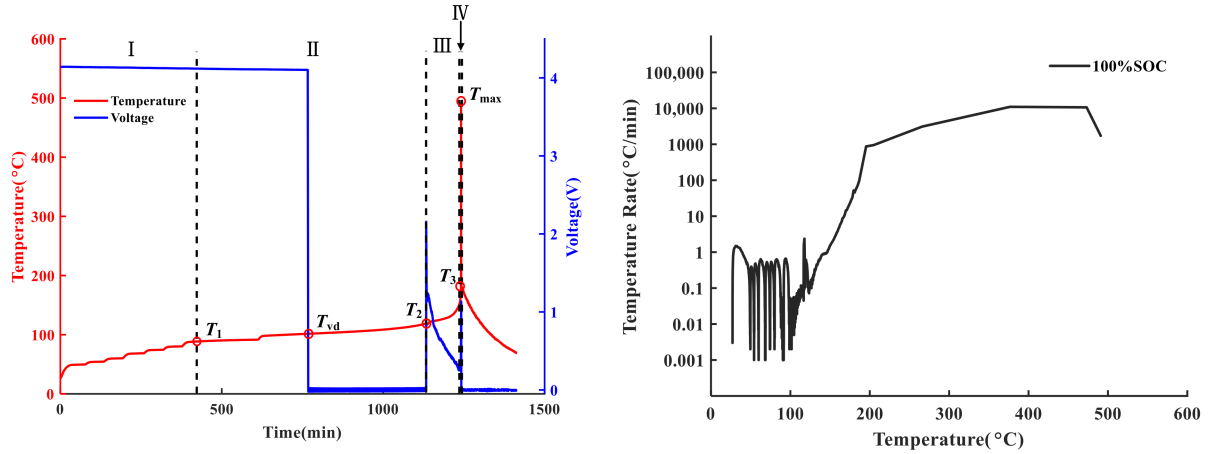
The temperature and voltage change curves of the batteries with different SOC conditions during the TR process are shown in Figure 6. It can be seen from the curves with 100% SOC in Figure 6a, that the TR processes could be divided into four stages with three critical temperatures.

Stage 1: The battery self-heating rate is less than the set value of  $0.02\text{ }^{\circ}\text{C}/\text{min}$ , and the EV+-ARC works in the H-W-S mode. The capacity of the battery decays at high temperatures and the voltage drops slightly [16].

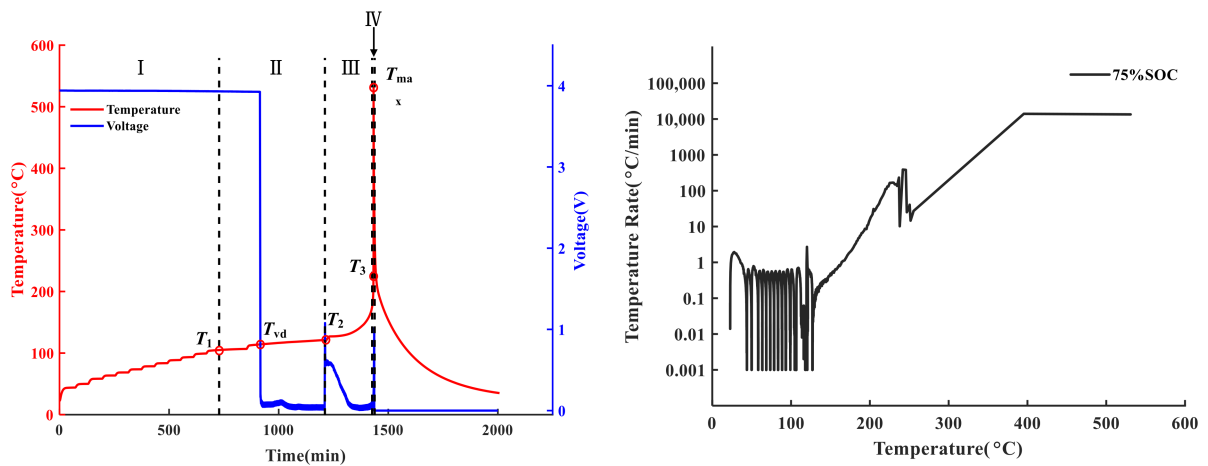
Stage 2:  $T_1$  is the temperature where EV+-ARC detects the self-heating of the battery, which is determined by the temperature rate sensitivity set value. Thereafter, EV+-ARC enters the exothermic mode from the Heat-Wait-Seek mode and starts to track the temperature change of the battery. In stage 2, the voltage of the battery drops sharply to around 0 V, and the corresponding temperature is represented by  $T_{vd}$  in Figure 6a. The solid electrolyte interface (SEI) decomposes as the temperature increases. In addition, the anode that has lost the protection of the SEI film starts to react with the electrolyte [22,23]. The heat released by the reaction leads the battery temperature to rise slowly.

Stage 3:  $T_2$  is the temperature where the battery safety vent opens. At higher temperature, various chemical reactions inside the battery will produce a large amount of gas, resulting in an increase in the internal pressure of the battery. When the internal pressure reaches the critical threshold, the safety vent will open to relieve the pressure [24]. As the gas is discharged, the temperature of the battery drops slightly. Then, the heat is released by the chemical reactions of the internal materials of the battery, such as the SEI decomposition,

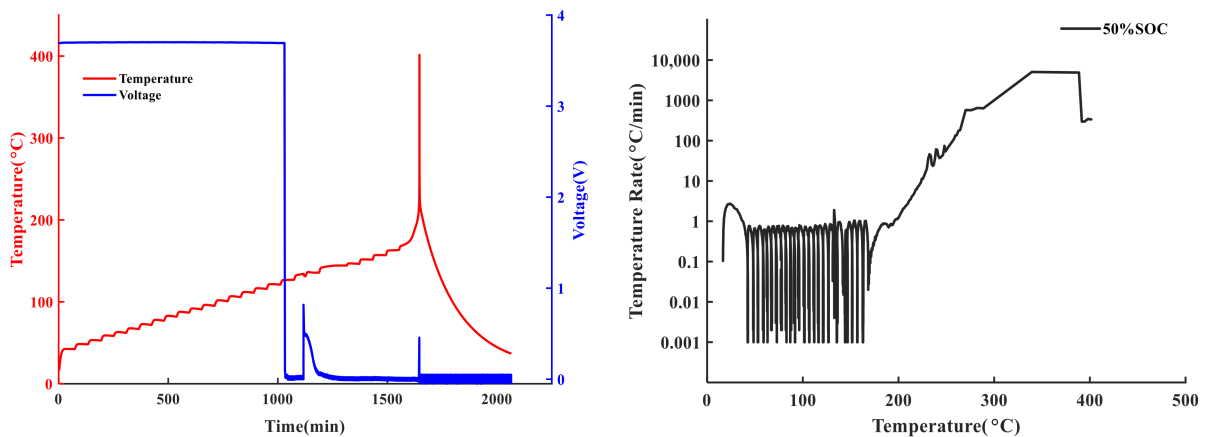
cathode decomposition, and anode reactions with the electrolyte, etc. [13,21,24], which will slowly increase the temperature of the battery again. Moreover, as the temperature rises, the chemical reaction rate further accelerates, and the battery temperature rises faster.



(a) Temperature and voltage variation curves of 100% SOC.



(b) Temperature and voltage variation curves of 75% SOC



(c) Temperature and voltage variation curves of 50% SOC

Figure 6. Cont.

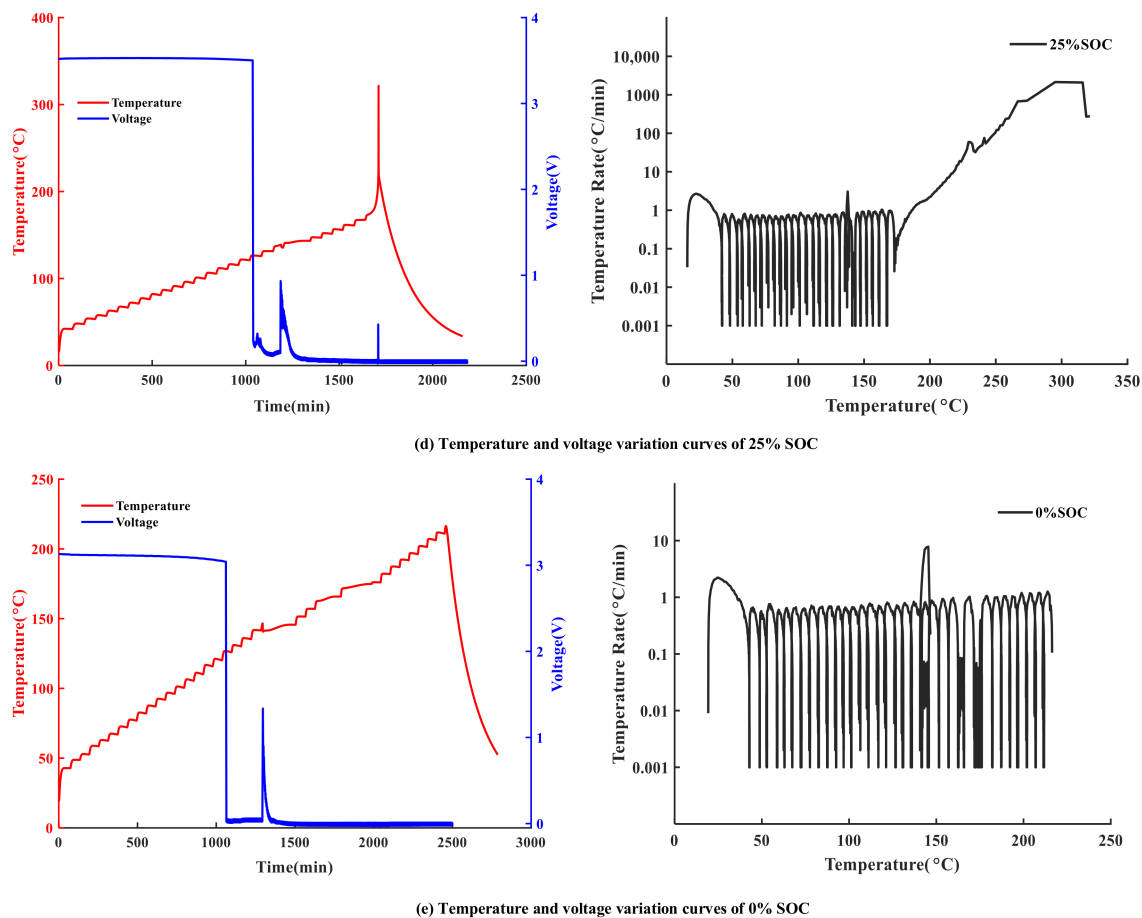


Figure 6. Temperature and voltage variation curves of different SOC batteries.

Stage 4:  $T_3$  is the critical temperature where the battery TR is triggered, defined as the  $T(t_1)$  when the difference between  $T(t_1)$  and  $T(t_2)$  is greater than  $1\text{ }^\circ\text{C/s}$  [16]. In stage 4, the internal chemical reaction of the battery intensifies, such as the decomposition reaction of the cathode, the reaction of the anode and the electrolyte, the decomposition reaction of the electrolyte, etc. [13,21,24,25], which will release a large amount of heat and cause the battery temperature to rise sharply.

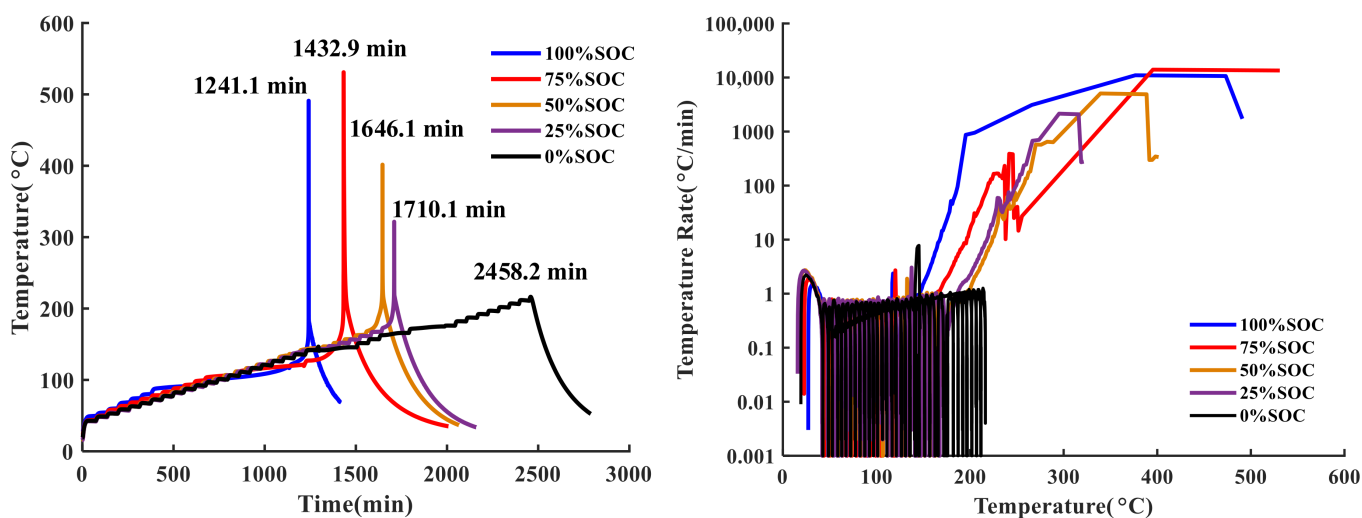
The anode material will undergo a variety of chemical reactions in the range of  $100\text{--}300\text{ }^\circ\text{C}$ , the graphite crystal structure will collapse and deform, and  $\text{LiC}_6$  and  $\text{Li}_x\text{Si}$  will react with the electrolyte and release heat [21]. The silicon, whether it is crystalline or amorphous, will be transformed into an amorphous phase and then into a crystalline compound in the lithium intercalation process [13,26]. In the temperature range of  $110\text{--}300\text{ }^\circ\text{C}$ , the cathode has experienced a series of phase transitions from a layered structure to a  $\text{M}_3\text{O}_4$  spinel to rock salt [21,27,28]. Both of these processes require the release of a large amount of oxygen, which reacts with the electrolyte and releases a large amount of heat.

### 3.2. Influence of Different SOC Conditions on the Harm of Battery Thermal Runaway

Figure 7a shows the curves of battery surface temperature with time under different SOC conditions. In general, with the decrease of SOC, the time increases from the beginning of the battery heating to the time the thermal runaway occurs. The time of thermal runaway in 75% SOC is about 191 min later than that in 100% SOC, and the time of thermal runaway in 50% SOC is about 214 min later than that in 75% SOC. At the same time, the higher the SOC, the higher the maximum surface temperature of the battery when the TR occurs. Figure 7b shows the temperature rise rate curves of the battery under different SOC conditions. It can be seen from Figure 6 that the maximum temperature rise rate of the battery decreases with the decrease of SOC. When SOC is 100%, the maximum temperature

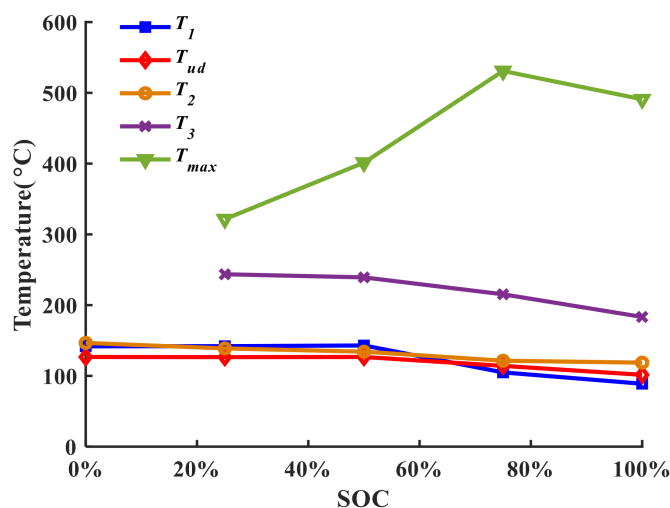
rise rate of the battery can reach about 10,000 °C/min, while the maximum temperature rise rate of the battery only is about 2000 °C/min in 25% SOC.

The various critical temperature data in the process of thermal runaway of the lithium-ion battery under different SOC conditions are summarized in Table 2, which is also shown in Figure 7c. When the battery enters the TR, the maximum temperature increases as the SOC increases. The self-heating starting temperature and the TR trigger the temperature decrease with the increase of SOC. The temperature when the safety vent is opened and the temperature when the voltage drops to 0 do not change much in the range of 0%~100% SOC, but a downward trend is still shown with the increase of SOC. This may be due to the fact that with the increase of SOC, the active materials in the battery are more prone to various chemical reactions, which generate a lot of heat and release more flammable gases. In addition, at 0% SOC, the battery does not trigger the TR.



(a) Temperatures of different SOC battery

(b) Temperatures rise rate of different SOC battery



(c) The critical temperature points of thermal runaway

Figure 7. The comparison of TR of different SOC batteries.

Figure 8 shows the appearance of the fresh battery and the battery under different SOC conditions after the TR. In containment systems, the high pressure generated by the gas released from the battery can damage the vent, and this effect is exacerbated as the SOC increases. At 100% and 75% SOC, the battery explodes, rupturing its container and

burning its shell. The electrolyte and some of the electrode material inside the battery eject from the positive electrode, thus the mass loss is higher than under the other conditions.



**Figure 8.** The photographs of the sample battery before and after the TR experiment.

**Table 2.** The main data after the adiabatic TR experiment for the battery under different SOC conditions.

SOC (%)	Mass (g)	Voltage (V)	$T_1$ (°C)	$T_{vd}$ (°C)	$T_2$ (°C)	$T_3$ (°C)	$T_{max}$ (°C)
0	47	3.13	141.8	126.7	146.6	-	-
25	47	3.52	142	126.5	138.8	243.6	321.5
50	47	3.69	143	126.7	134.2	239.2	401.4
75	47	3.94	104.8	114.1	121.4	215.3	530.9
100	47	4.14	88.9	101.5	118.7	183.3	490.9

### 3.3. Energy Calculation and Conversion

The thermal explosion is the most dangerous condition in an adiabatic condition. Therefore, in this case, the research is very important for the safety considerations of the actual research. First, based on the EV+-ARC experimental data and battery mass, specific heat capacity, and transient temperature distribution, the total energy released by the battery in the process of adiabatic TR can be calculated in this study. The calculation method is shown in (3).

$$\Delta H = mc_p(T_{max} - T_3) \quad (3)$$

where  $\Delta H$  represents the total energy released from the battery,  $c_p$  represents the specific heat capacity of the battery, which is 1020 J/kg/K measured by the EV+-ARC,  $m$  represents the mass of the battery, which is 47 g,  $T_{max}$  represents the maximum temperature of the battery surface,  $T_3$  represents the trigger temperature of battery TR.

The investigation of explosion and energy release is very significant for the conversion between TNT and other explosives, and TNT is one of the components of commonly used explosives. The thermal runaway reaction of lithium-ion batteries can also be seen as one type of explosion. In order to intuitively explain the energy released by the lithium-ion battery during thermal runaway, the TNT equivalent method is used to convert its thermal energy into the TNT equivalent, which is shown in (4) [29,30]. The calculation results are shown in Table 3.

$$W = \eta \Delta H / H_{TNT} \quad (4)$$

where  $W$  represents the mass of TNT (TNT-equivalent), which is transferred from the thermal energy to the mass of TNT.  $\eta$  represents the explosive efficiency of the material, in which the thermal energy of the battery can be calculated from (3), thus  $\eta$  can be set to 1.  $H_{TNT}$  represents the explosive energy of TNT, which varies from 4437 to 4765 kJ/kg. In this paper, the value of  $H_{TNT}$  is 4500 kJ/kg.

**Table 3.** The values of the energy and TNT-equivalent for the battery at different SOC conditions.

SOC (%)	$T_3$ (°C)	$T_{max}$ (°C)	$\Delta H$ (kJ)	TNT-Equivalent (g)
100	183.3	490.9	14.75	3.28
75	215.3	530.9	15.13	3.36
50	239.2	401.4	7.78	1.73
25	243.6	321.5	3.73	0.83

#### 4. Conclusions

In this article, the TR hazard of nickel-rich 18650 lithium-ion batteries with different SOC conditions is studied through the adiabatic calorimetry experiment using EV+-ARC. All the batteries are charged to the specific SOC, and then they are put into the EV+-ARC to be heated until self-heating is detected. Eventually, the battery triggers the TR under adiabatic conditions. In order to evaluate the TR characteristics, some characteristic parameters such as battery voltage, surface temperature, temperature rise rate, etc. are selected from the experiment to analyze the influence of SOC on the critical state of TR.

The adiabatic TR experiment shows that the TR risk of 18650 lithium-ion batteries increases with the increase of SOC. For the lithium-ion battery with 100% SOC, the self-heating starting temperature is 88.9 °C, the trigger temperature of TR is 183 °C, and the maximum temperature of the battery surface is about 490.9 °C. The explosion causes the battery's steel shell to rupture and release 14.75 kJ of thermal energy, which is equivalent to 3.28 g TNT. For the lithium-ion battery with 25% SOC, the self-heating temperature increases to 142 °C, the trigger temperature of the TR increases to 243.6 °C, and the maximum surface temperature decreases to about 321 °C. The temperature when the safety vent is opened and the temperature when the voltage drops to 0 do not change much in the range of 0%~100% SOC, but it still shows a downward trend with the increase of SOC. Moreover, as the SOC decreases, the delay time of the self-heating reaction and TR increases. Furthermore, at 0% SOC, the battery does not trigger the TR.

**Author Contributions:** Conceptualization, K.J., P.G. and P.H.; methodology, K.J. and P.H.; investigation, K.J. and P.H.; design of the experiments, K.J., P.G. and P.H.; software, K.J. and P.H.; data analysis, Y.Z. and P.H.; writing—original draft preparation, K.J.; writing—review, editing, and providing some valuable suggestions, P.G., Y.Z. and B.D.; project administration, B.D. and C.Z.; funding acquisition, B.D. and C.Z. All authors contributed to this work. All authors have read and agreed to the published version of the manuscript.

**Funding:** This paper is supported by the National Natural Science Foundation of China (no. U1964207, 62133007, U1764258, U1864205), and the Key research and development program of China (no. 2018YFB0104000).

**Conflicts of Interest:** The authors declare no conflict of interest.

## Abbreviations

The following abbreviations are used in this manuscript:

TR	thermal runaway
SOC	state of charge
EV+-ARC	extended volume plus acceleration calorimeter
VSP2	vent sizing package 2
LCO	LiCoO <sub>2</sub>
LMO	LiMnO <sub>2</sub>
LFP	LiFePO <sub>4</sub>
NCM111	Li[Ni <sub>1/3</sub> Co <sub>1/3</sub> Mn <sub>1/3</sub> ]O <sub>2</sub>
NCM622	Li[Ni <sub>0.6</sub> Co <sub>0.2</sub> Mn <sub>0.2</sub> ]O <sub>2</sub>
NCM811	Li[Ni <sub>0.8</sub> Co <sub>0.1</sub> Mn <sub>0.1</sub> ]O <sub>2</sub>
EVs	electric vehicles
BMS	battery management system
EV-ARC	extended volume acceleration rate calorimeter
DSC	differential scanning calorimeter
DC	direct current
CC-CV	constant current-constant voltage
H-W-S	heat-wait-see
SEI	solid electrolyte interface

## References

- Duan, B.; Zhang, Q.; Geng, F.; Zhang, C. Remaining useful life prediction of lithium-ion battery based on extended Kalman particle filter. *Int. J. Energy Res.* **2019**, *44*, 1724–1734. [[CrossRef](#)]
- Duan, B.; Li, Z.; Gu, P.; Zhou, Z.; Zhang, C. Evaluation of battery inconsistency based on information entropy. *J. Energy Storage* **2018**, *16*, 160–166. [[CrossRef](#)]
- Shan, X.-Y.; Li, F.; Wang, D.-W.; Cheng, H.-M. The smart era of electrochemical energy storage devices. *Energy Storage Mater.* **2016**, *3*, 66–68. [[CrossRef](#)]
- Cano, Z.P.; Banham, D.; Ye, S.; Hintennach, A.; Lu, J.; Fowler, M.; Chen, Z. Batteries and fuel cells for emerging electric vehicle markets. *Nat. Energy* **2018**, *3*, 279–289. [[CrossRef](#)]
- Julien, C. Design Considerations for Lithium Batteries. In *Materials for Lithium-ion Batteries*; Julien, C., Stoyanov, Z., Eds.; Kluwer Academic Publishers: Dordrecht, The Netherlands, 2000; pp. 1–20. [[CrossRef](#)]
- Yoshio, M.; Noguchi, H. A review of positive electrode materials for lithium-ion batteries. In *Lithium-ion Batteries*; Yoshio, M., Brodd, R.J., Kozawa, A., Eds.; Springer: New York, NY, USA, 2009; pp. 31–33.
- Ehrlich, G.M. Lithium-ion batteries. In *Handbook of Batteries*, 3rd ed.; Reddy, T.B., Linden, D., Eds.; McGraw-Hill: New York, NY, USA, 2002; pp. 35.1–35.94.
- Schipper, F.; Erickson, E.M.; Erk, C.; Shin, J.-Y.; Chesneau, F.F.; Aurbach, D. Review-Recent advances and remaining challenges for lithium ion battery cathodes I. Nickel-rich, LiNixCoyMnzO<sub>2</sub>. *J. Electrochem. Soc.* **2017**, *164*, A6220–A6228. [[CrossRef](#)]
- Jiang, K.; Wang, T.; Li, X.; Duan, B.; Zhang, C. Simulation of Thermal Runaway Prediction Model for Nickel-Rich Lithium-ion Batteries. In Proceedings of the 2020 Chinese Automation Congress, Shanghai, China, 6–8 November 2020.
- Wang, Q.; Ping, P.; Zhao, X.; Chu, G.; Sun, J.; Chen, C. Thermal runaway caused fire and explosion of lithium ion battery. *J. Power Sources* **2012**, *208*, 210–224. [[CrossRef](#)]
- Lyon, R.E.; Walters, R.N. Energetics of lithium ion battery failure. *J. Hazard. Mater.* **2016**, *318*, 164–172. [[CrossRef](#)] [[PubMed](#)]
- Wen, J.; Yu, Y.; Chen, C. A Review on Lithium-Ion Batteries Safety Issues: Existing Problems and Possible Solutions. *Mater. Express* **2012**, *2*, 197–212. [[CrossRef](#)]
- Li, H.; Kong, X.; Liu, C.; Zhao, J. Study on thermal stability of nickel-rich/silicon-graphite large capacity lithium ion battery. *Appl. Therm. Eng.* **2019**, *161*, 114144. [[CrossRef](#)]
- Jhu, C.-Y.; Wang, Y.-W.; Shu, C.-M.; Chang, J.-C.; Wu, H.-C. Thermal explosion hazards on 18650 lithium ion batteries with a VSP2 adiabatic calorimeter. *J. Hazard. Mater.* **2011**, *192*, 99–107. [[CrossRef](#)] [[PubMed](#)]
- Feng, X.; Ouyang, M.; Liu, X.; Lu, L.; Xia, Y.; He, X. Thermal runaway mechanism of lithium ion battery for electric vehicles: A review. *Energy Storage Mater.* **2017**, *10*, 246–267. [[CrossRef](#)]
- Feng, X.; Fang, M.; He, X.; Ouyang, M.; Lu, L.; Wang, H.; Zhang, M. Thermal runaway features of large format prismatic lithium ion battery using extended volume accelerating rate calorimetry. *J. Power Sources* **2014**, *255*, 294–301. [[CrossRef](#)]
- Wang, Q.; Sun, J.; Chen, X.; Chu, G.; Chen, C. Effects of solvents and salt on the thermal stability of charged LiCoO<sub>2</sub>. *Mater. Res. Bull.* **2009**, *44*, 543–548. [[CrossRef](#)]
- Jiang, L.; Wang, Q.; Sun, J. Electrochemical performance and thermal stability analysis of LiNixCoyMnzO<sub>2</sub> cathode based on a composite safety electrolyte. *J. Hazard. Mater.* **2018**, *351*, 260–269. [[CrossRef](#)] [[PubMed](#)]

19. Mao, B.; Chen, H.; Cui, Z.; Wu, T.; Wang, Q. Failure mechanism of the lithium ion battery during nail penetration. *Int. J. Heat Mass Transf.* **2018**, *122*, 1103–1115. [[CrossRef](#)]
20. Ren, D.; Feng, X.; Lu, L.; Ouyang, M.; Zheng, S.; Li, J.; He, X. An electrochemical-thermal coupled over-charge-to-thermal-runaway model for lithium ion battery. *J. Power Sources* **2017**, *364*, 328–340. [[CrossRef](#)]
21. Liu, C.; Li, H.; Kong, X.; Zhao, J. Modeling analysis of the effect of battery design on internal short circuit hazard in  $\text{LiNi}_{0.8}\text{Co}_{0.1}\text{Mn}_{0.1}\text{O}_2/\text{SiOx}$ -graphite lithium ion batteries. *Int. J. Heat Mass Transf.* **2020**, *153*, 119590. [[CrossRef](#)]
22. Ryou, M.-H.; Lee, J.-N.; Lee, D.J.; Kim, W.-K.; Jeong, Y.K.; Choi, J.W.; Park, J.-K.; Lee, Y.M. Effects of lithium salts on thermal stabilities of lithium alkyl carbonates in SEI layer. *Electrochim. Acta* **2012**, *83*, 259–263. [[CrossRef](#)]
23. Yang, H.; Shen, X.-D. Dynamic TGA-FTIR studies on the thermal stability of lithium/graphite with electrolyte in lithium-ion cell. *J. Power Sources* **2007**, *167*, 515–519. [[CrossRef](#)]
24. Mao, B.; Huang, P.; Chen, H.; Wang, Q.; Sun, J. Self-heating reaction and thermal runaway criticality of the lithium ion battery. *Int. J. Heat Mass Transf.* **2019**, *149*, 119178. [[CrossRef](#)]
25. Bak, S.-M.; Hu, E.; Zhou, Y.; Yu, X.; Senanayake, S.; Cho, S.-J.; Kim, K.-B.; Chung, K.Y.; Yang, X.-Q.; Nam, K.-W. Structural Changes and Thermal Stability of Charged  $\text{LiNi}_x\text{Mn}_y\text{Co}_z\text{O}_2$  Cathode Materials Studied by Combined In Situ Time-Resolved XRD and Mass Spectroscopy. *ACS Appl. Mater. Interfaces* **2014**, *6*, 22594–22601. [[CrossRef](#)] [[PubMed](#)]
26. Wang, C.-M.; Li, X.; Wang, Z.; Xu, W.; Liu, J.; Gao, F.; Kovarik, L.; Zhang, J.-G.; Howe, J.; Burton, D.J.; et al. In situ TEM investigation of congruent phase transition and structural evolution of nanostructured silicon/carbon anode for lithium ion batteries. *Nano Lett.* **2012**, *12*, 1624–1632. [[CrossRef](#)] [[PubMed](#)]
27. Li, Y.; Liu, X.; Wang, L.; Feng, X.; Ren, D.; Wu, Y.; Xu, G.; Lu, L.; Hou, J.; Zhang, W.; et al. Thermal runaway mechanism of lithium-ion battery with  $\text{LiNi}_{0.8}\text{Mn}_{0.1}\text{Co}_{0.1}\text{O}_2$  cathode materials. *Nano Energy* **2021**, *85*, 105878. [[CrossRef](#)]
28. Tsukasaki, H.; Fukuda, W.; Morimoto, H.; Arai, T.; Mori, S.; Hayashi, A.; Tatsumisago, M. Thermal behavior and microstructures of cathodes for liquid electrolyte-based lithium batteries. *Sci. Rep.* **2018**, *8*, 15613. [[CrossRef](#)]
29. Lu, T.-Y.; Chiang, C.-C.; Wu, S.-H.; Chen, K.-C.; Lin, S.-J.; Wen, C.-Y.; Shu, C.-M. Thermal hazard evaluations of 18650 lithium-ion batteries by an adiabatic calorimeter. *J. Therm. Anal. Calorim.* **2013**, *114*, 1083–1088. [[CrossRef](#)]
30. Chen, W.-C.; Wang, Y.-W.; Shu, C.-M. Adiabatic calorimetry test of the reaction kinetics and self-heating model for 18650 Li-ion cells in various states of charge. *J. Power Sources* **2016**, *318*, 200–209. [[CrossRef](#)]